

Initial set of oceanographic data from Bay of Bengal using an underwater glider as mobile sensor node

Shijo Zacharia^{1,2,*}, R. Seshasayanan², V. Gowthaman¹, S. Muthukumaravel¹, Tata Sudhakar¹ and M. A. Atmanand¹

¹National Institute of Ocean Technology, Ministry of Earth Sciences, Pallikaranai, Chennai 600 100, India

²College of Engineering, Guindy Campus, Anna University, Chennai 600 025, India

Underwater gliders measure high-resolution spatio-temporal oceanographic data. However, glider operations have not been carried out in the Indian Ocean region so far. In September 2013, the National Institute of Ocean Technology, Chennai introduced a mobile sensor node, the underwater glider ‘Barathi’, for observation in the Bay of Bengal (BoB). Herein we address ballasting procedure of the glider operated in highly variable density waters of the BoB. The temperature and conductivity data collected by us are strongly correlated with commercially available instrument with coefficient of determination $R^2 > 0.97$. This article reports results from a long-duration (127 days) mission in 2014. The variation of temperature, salinity, density, sound velocity, mixed layer depth, sonic layer depth and lower cutoff frequency of surface duct along 13°N lat. and between 80.76°E and 86.28°E long. are also presented. The results show a trace of the East Indian Coastal Current. The glider operations demonstrate a novel *in situ* observation platform in the BoB.

Keywords: Mobile sensor node, oceanographic data, underwater glider, underwater acoustics.

CHALLENGES still exist in understanding the nature of the ocean and its spatio-temporal variation. *In situ* observations are made in the Indian Ocean region by means of deep sea current meter mooring arrays¹, data buoys^{2,3}, Research moored array for African–Asian–Australian monsoon analysis and prediction (RAMA) buoys⁴, drifter buoys, expendable bathythermograph (XBT)⁵, Ship on Opportunity Programme (SOOP)⁶ and Array for real-time geostrophic oceanography (Argo) profiling floats⁷. The Bay of Bengal (BoB) in the northern summer is the site of highest mean precipitation of the global oceans⁸. The East Indian Coastal Current (EICC) and presence of eddies are the major features of circulation in the BoB⁹. Therefore, detailed sampling and research in the BoB is important¹⁰.

Underwater gliders are now considered as vital platforms for high-resolution *in situ* ocean observation¹¹.

Gliders are unmanned autonomous underwater vehicles with variable buoyancy^{12–15}. The first underwater glider flight trials began in 1992 at Webb Research Corporation, East Falmouth, USA¹⁶. The first glider sea trials were conducted with a Slocum glider in a New Jersey site in July 1998 (refs 17 and 18). In 2009, a glider voyaged 7400 km in 221 days and crossed the Atlantic Ocean¹⁹. Details of commercially available underwater gliders are given in Table 1 (refs 20–26). The unique features of the Slocum electric glider are operating depth (1000 m), horizontal speed (0.35 m/s), small size and Iridium communication system with global range. Only a few technical groups in the world manufacture and operate underwater gliders²⁷. However, gliders have not been operated in the Indian Ocean so far^{28–30}. The buoyancy-driven underwater vehicles encounter difficulty in the BoB due to density and temperature variation. The buoyancy-driven Argo floats failed to surface when the density of the float was greater than the environmental density^{31–33}.

In this scenario, in September 2013 the National Institute of Ocean Technology (NIOT), Chennai introduced a mobile sensor node, an underwater glider for high spatio-temporal resolution measurement in the BoB. The present study reports ballasting procedure of a ‘Slocum G2 glider’ ‘Barathi’ (manufactured by Teledyne Webb Research, USA) for long-duration operation and results from its missions over the BoB in September 2013 and April–August 2014. This article provides a comparison of temperature and conductivity measurements of glider Barathi with commercially available instruments. The variation of temperature, density, salinity, sound velocity, mixed layer depth, sonic layer depth and lower cutoff frequency of surface duct along 13°N lat. and between 80.76° and 86.28°E long. are also presented.

Means and methods

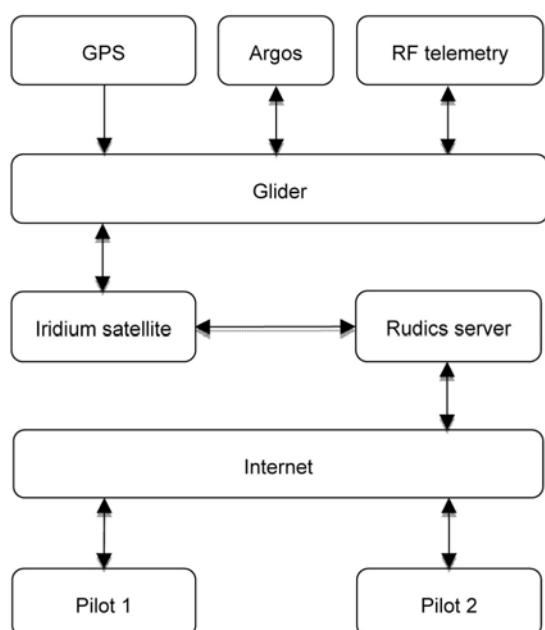
Glider Barathi

The glider hull has three dry sections and two wet sections¹⁷. Two wings which sweep backwards are attached

*For correspondence. (e-mail: zacharia@niot.res.in)

Table 1. Details of commercially available underwater gliders

Parameters	Slocum electric ²⁰⁻²²	Slocum thermal ²²	Sea glider ²³	Sea explorer ²⁴	Spray ^{25,26}
Hull	Length 1.52 m, diameter 0.21 m	Length 3.2 m, diameter 0.21 m	Length 1.8 m, diameter 0.3 m	Length 2 m, diameter 0.25 m	Length 2.13 m, diameter 0.2 m
Battery-type	Alkaline, lithium primary	Alkaline	Lithium primary	Rechargeable lithium ion	Lithium primary
Drive method	Volume change $520 \times 10^{-4} \text{ m}^3$	Buoyancy change $\pm 50 \text{ g}$	Volume change $841 \times 10^{-4} \text{ m}^3$	Volume change $1000 \times 10^{-4} \text{ m}^3$	Volume change $700 \times 10^{-4} \text{ m}^3$
Maximum operating depth (m)	200, 1000 (for G2 model)	2600	1000	700	1500
Endurance	2300 km	40,000 km	4600 km	1200 km/2 months	4800 km/6 months
Horizontal speed (m/s)	0.35	0.4	0.25	0.5	0.27
Communication	Short range radio, frequency, Iridium, Advanced Research and Global Observation Satellite (Argos)	Radio frequency local area network	Iridium	Short-range radio frequency, Iridium	Iridium, Argos

**Figure 1.** Assembled glider.**Figure 2.** Overview of communication system.

on both sides of the mid hull section. The forward dry hull assembly houses ballast pump, pitch vernier and forward batteries. The ballast pump moves oil from an internal reservoir to an external bladder to change buoyancy. The forward battery position controls pitch angle. A conductivity and temperature profiler (Sea-bird, USA), single wavelength light scatter sensor (Wet Labs, USA), and combo flurometer–turbidity sensor (Wet Labs, USA) are integrated in the mid dry hull section. The aft dry hull section houses mission controller electronics, attitude sensor, communication electronics, battery pack, pressure sensor and air pump. An external oil bladder ($2.6 \times 10^{-4} \text{ m}^3$) is assembled in the forward wet section. Figure 1 shows a photograph of an assembled glider. The communication system (Figure 2) of the glider contains Argos satellite platform terminal, global position system (GPS) receiver, Iridium satellite telemetry modem, and a radio frequency (RF) transceiver with 1 km range. The glider communicates from remote locations through the Iridium satellite telemetry to rudics server (at Teledyne Webb Research Corporation, USA). The pilots communicate to the glider through the rudics server.

For a neutrally buoyant underwater glider, increase in volume reduces its density and results in positive buoyancy. Similarly, decrease in volume of the glider increases its density and results in negative buoyancy. The buoyancy and attitude result in the generation of hydrodynamic lift and drag forces on the wings and body of the glider. A preprogrammed value of buoyancy (± 2.6 N) and pitch ($\pm 26^\circ$) aid the glider to slide along vertically and voyage horizontally and efficiently.

Ballasting

Ballasting procedure changes mass of the glider prior to deployment to improve stability and limit buoyancy in sea-water condition. The total mass of the glider was adjusted by changing mass in ballast bottles ($6 \times 10^{-5} \text{ m}^3$) at forward and aft ends, mass of stainless steel plates on both ends of the science payload or mass on wing rails.

Initially the glider was immersed in a water tank (3 m \times 2 m \times 1 m) and the conductivity and temperature of water were measured. The glider was programmed to empty oil bladder, deflate airbladder and set attitude with 0° pitch and 0° roll. The glider was suspended in water on two load cells and measured the weight. The glider mass was changed gradually to achieve neutral buoyancy condition. A properly ballasted glider for tank water condition surfaced with waterline on the digital tail fin (Figure 3).

The glider mass needs to be adjusted to achieve neutral buoyancy condition for a long-duration mission in the BoB. The salinity of the BoB varies due to large influx of freshwater from river discharge, precipitation and high amount of rainfall. Wind, the main forcing function over the Indian Ocean, reverses direction twice in a year. The EICC reverses direction twice a year, flowing northeastward from February until September with a strong peak in March–April and southwest ward from October to January with strongest flow in November³⁴. These reversing currents carry high saline Arabian Sea water into the BoB and vice versa^{2,3,35–38}. The density variations



Figure 3. A properly ballasted glider for tank water.

result from the above processes and variations in sea surface temperature (SST) are the major challenges for buoyancy-driven gliders in the BoB^{39,40}. The mass of the glider was adjusted by considering the density and SST variations as described below.

We studied the sea surface (5 m depth) mean temperature (Figure 4) and salinity of the region 12.66° – 13.10° N by 81.04° – 92.20° E for the months April–June in 2003–2011 from Argo’s historical data⁴¹. The sea-surface mean density (Figure 5) was computed from 10-days averaged surface salinity and temperature data using eq. (1) below.

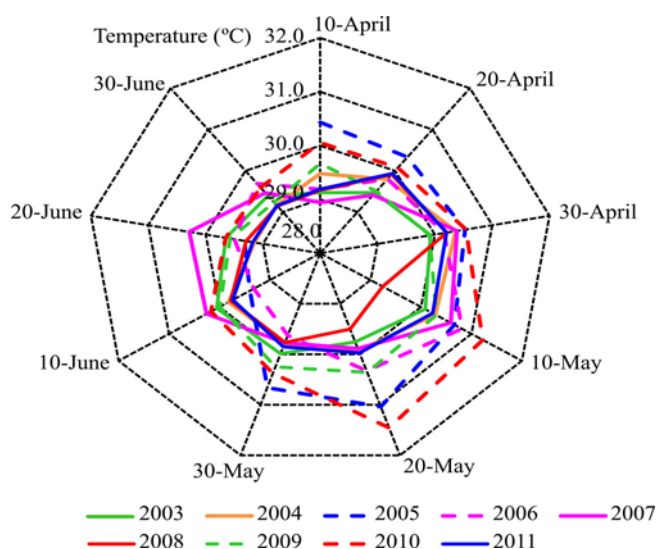


Figure 4. Sea-surface mean temperature for the months of April–June in 2003–2011.

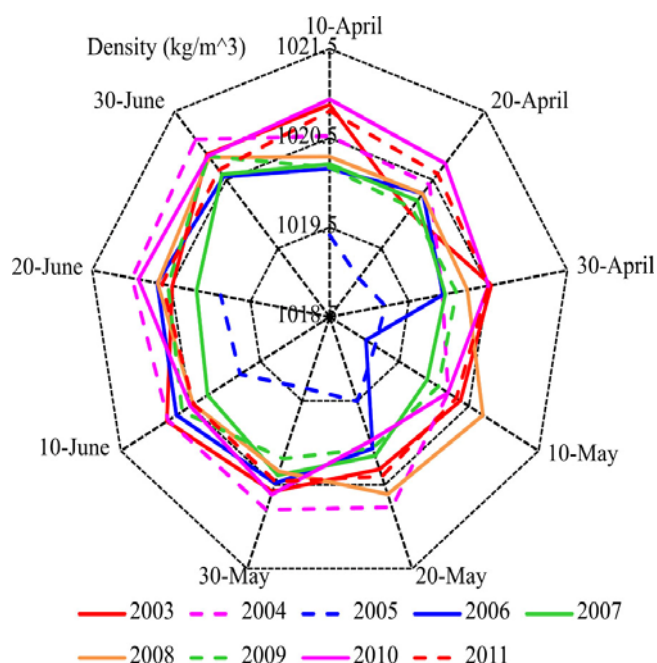


Figure 5. Sea-surface mean density for the months of April–June in 2003–2011.

The density of standard sea water (ρ_{sw}) is given by

$$\rho_{sw} = \rho_0 + AS + BS^{1.5} + CS^2, \quad (1)$$

where ρ_0 is the density of pure water, S the salinity of sea water and the coefficients A , B and C are functions of temperature⁴²⁻⁴⁴. The coefficients A , B and C are given by

$$\begin{aligned} A &= 8.24493 \times 10^{-1} - 4.0899 \times 10^{-3} T \\ &+ 7.6438 \times 10^{-5} T^2 - 8.2467 \times 10^{-7} T^3 \\ &+ 5.3875 \times 10^{-9} T^4, \end{aligned} \quad (2)$$

$$\begin{aligned} B &= -5.72466 \times 10^{-3} + 1.0227 \times 10^{-4} T \\ &+ 1.6546 \times 10^{-6} T^2, \end{aligned} \quad (3)$$

$$C = 4.8314 \times 10^{-4}. \quad (4)$$

The density of pure water is given by

$$\begin{aligned} \rho_0 &= 999.842594 + 6.793952 \times 10^{-2} T \\ &- 9.095290 \times 10^{-3} T^2 + 1.001685 \times 10^{-4} T^3 \\ &- 1.120083 \times 10^{-6} T^4 + 6.536332 \times 10^{-9} T^5, \end{aligned} \quad (5)$$

where T is the temperature of water.

The change in weight (w) on account of SST and density variations was calculated using eq. (6) as follows

$$w = D_g [\alpha_g \rho_{sw} (T_{sw} - T_{tw}) + (\rho_{sw} - \rho_{tw})], \quad (6)$$

where D_g is the total displacement of the glider ($56.3 \times 10^{-3} \text{ m}^3$), α_g the thermal coefficient of the glider (53.5×10^{-6}), ρ_{sw} the sea-surface mean density, T_{sw} the sea-surface mean temperature, T_{tw} the temperature of water in the ballast tank (30.2914°C), and ρ_{tw} is the density of ballast tank water (1018.0670 kg/m^3).

The change in weight (w) of the glider deployed in the BoB was calculated using eq. (6) by substituting sea-surface mean density ($\rho_{sw} = 1020.3 \text{ kg/m}^3$) and surface temperature ($T_{sw} = 29.879^\circ\text{C}$). The weight ($w = 127 \times 10^{-3} \text{ kg}$) was distributed internally without affecting attitude of the vehicle. The parameters (ρ_{sw} , T_{sw}) were verified with Argo data (platform no. 2901288 cycle no. 253 on 17 April 2014 at position 13.387°N 84.496°E , sea-surface mean temperature $T_{sw} = 30.142^\circ\text{C}$, sea-surface mean salinity = 33.068 psu)⁴⁵. The difference in weight was $6 \times 10^{-3} \text{ kg}$ in the above cases.

Meta-centric height

The neutrally buoyant glider was immersed in the water tank at zero moment state after ballasting for tank water. The ballast weight was moved for a known distance towards the nose dome along the horizontal axis and

change in pitch was measured. The meta-centric height (h) was calculated using eq. (7) as follows^{46,47}

$$h = \frac{w_b \times \delta l}{D_g \times \rho_{tw} \times \tan \delta \theta}, \quad (7)$$

where w_b is the ballast weight, δl the displacement of ballast weight, D_g the total displacement of the glider, ρ_{tw} the density of ballast tank water and $\delta \theta$ is the measured pitch angle.

The meta-centric height ($5.27 \times 10^{-3} \text{ m}$) was calculated from the above measurement.

Mixed layer depth

The wave action and turbulence agitate the water near the surface and form a mixed layer. Density was calculated from the interpolated temperature, pressure and conductivity data from the glider⁴⁴. Mixed layer depth (MLD) is defined as the depth at which the density is greater than the surface by 0.125 kg m^{-3} (refs 48, 49).

Sonic layer depth

The sound velocity was computed as reported by Fofonoff *et al.*⁵⁰ from the conductivity, temperature and pressure data measured by the glider. The salinity profile was computed from conductivity, temperature and pressure data from the glider⁴⁴. The sonic layer depth (SLD) for each profile was computed as near-surface first maximum in sound velocity profile (SVP)^{51,52}.

The surface duct is bound above by the sea surface and below by the SLD⁵³. The sound rays alternately refract and reflect within the surface duct. The sound wave attenuation in the surface duct is much less than normal spherical spreading. The maximum wavelength (λ_{\max}) of sound wave trap in the surface duct zone was estimated as follows

$$\lambda_{\max} = 8.51 \times 10^{-3} H^{3/2}, \quad (8)$$

where H is the height of the surface duct.

Assuming the velocity of sound as 1500 m/s , the minimum cut-off frequency (f_{\min}) of the surface duct was computed by

$$f_{\min} = 1.76 \times 10^5 H^{-3/2}. \quad (9)$$

Ocean surface current analyses real-time

The circulation features and wind of the region during the period were studied from the ocean surface current analyses real-time (OSCAR) forecast⁵⁴. Here, reference for direction is north to south and clockwise rotation is

positive. The forecast gives five days of temporal resolution and 1/3 degree of spatial resolution for surface current, in the case of wind, it is 3 h.

Advanced very high resolution radiometer

The daily mean SST from advanced very high resolution radiometer (AVHRR) data over the region on 27 April, 5 May and 3 June 2014 were analysed to interpret the results⁵⁵.

Results and discussion

Short-duration mission

Trajectory: The Barathi glider was deployed from aft of Ocean Research Vessel (ORV) *Sagar Manjusha* at position 12.8714°N, 84.0434°E on 13 September 2013 at 7:00 h (GMT) in 3300 m ocean depth. An RF antenna and fleet broadband antenna (Sailor 150, Thrane and Thrane, USA) were installed on the ship. The glider was

piloted through RF telemetry in a sequence of missions with dive depth of 100, 500 and 1000 m till 15 September 2013. The glider was also monitored through Iridium satellite telemetry. Figure 6 shows the trajectory of the glider. The glider was recovered with an inflatable boat launched from the ship.

Mission computer results: The mission computer on the glider measured depth, heading, pitch, battery position, roll, tail fin angle, internal vacuum and battery voltage on each dive. The following section depicts a mission at 12:45 h on 13 September 2013 at position 12.870°N, 84.0412°E.

The glider was commanded with the mission to dive to 950 m depth with 90° heading, -26° pitch angle and -2.6°N buoyancy variations. Figure 7 shows the time series of volume of oil in the external bladder. The internal battery was moved to 0.0114 m and generated -29.4° pitch. Figures 8 and 9 show the time series of battery

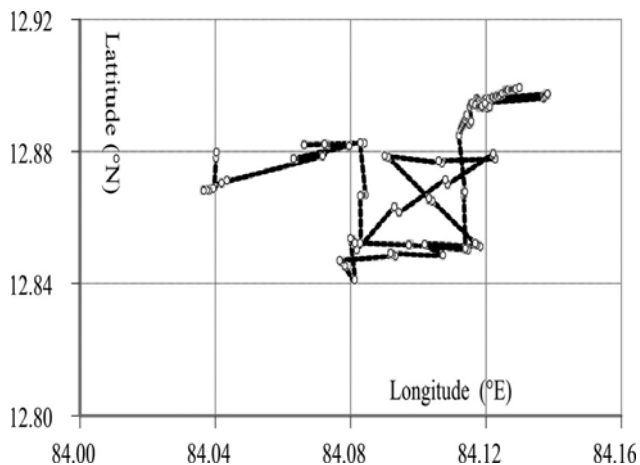


Figure 6. Trajectory of the Barathi during 13–15 September 2013.

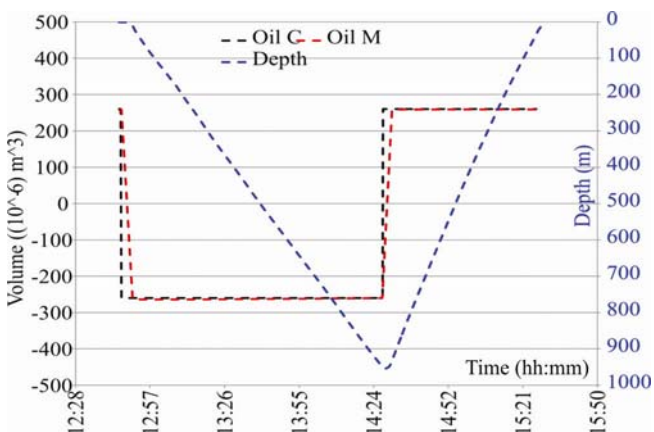


Figure 7. Commanded oil volume (Oil C), measured oil volume (Oil M) and depth (Depth) during the mission on 13 September 2013.

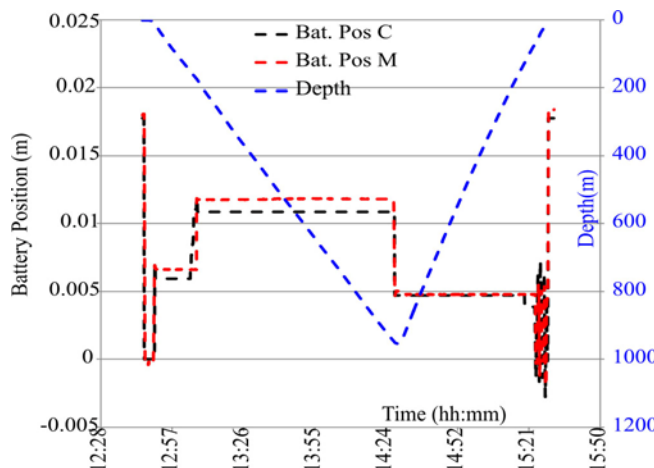


Figure 8. Commanded battery position (Bat. Pos C), measured battery position (Bat. Pos M), and depth (Depth) during the mission on 13 September 2013.

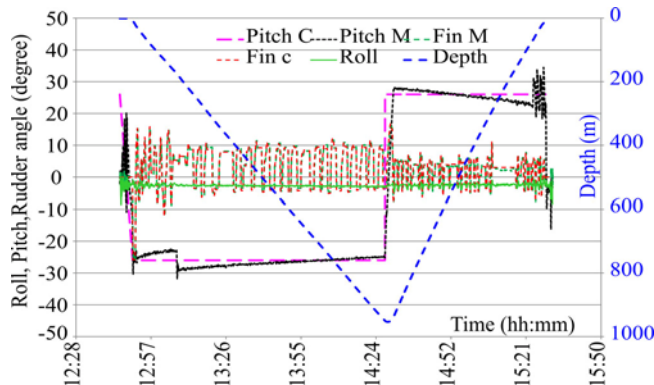


Figure 9. Commanded pitch (Pitch C), measured pitch (Pitch M), commanded rudder angle (Fin c), measured rudder angle (Fin M), measured roll (Roll) and depth (Depth) during the mission on 13 September 2013.

Table 2. Temperature and conductivity profiles

Profile	Time, date	Position	Measuring depth (m)
Barathi 1 (B1)	03 : 31, 15 September 2013	12.8974°N, 84.1383°E	1–99
Ship cast 1 (S1)	09 : 30, 16 September 2013	12.8629°N, 84.0442°E	1–99
Barathi 2 (B2)	07 : 53, 15 September 2013	12.8973°N, 84.1380°E	10–480
Ship cast 2 (S2)	09 : 30, 16 September 2013	12.8629°N, 84.0442°E	10–480

Table 3. Mean and standard deviation (SD) of temperature and conductivity profiles

Variable	Temperature (°C)		Conductivity (S/m)	
	Mean	SD	Mean	SD
Profile				
B1	24.55	3.10	5.200	0.255
S1	24.24	3.28	5.157	0.264
B2	15.01	5.38	4.303	0.506
S2	14.99	5.24	4.299	0.487

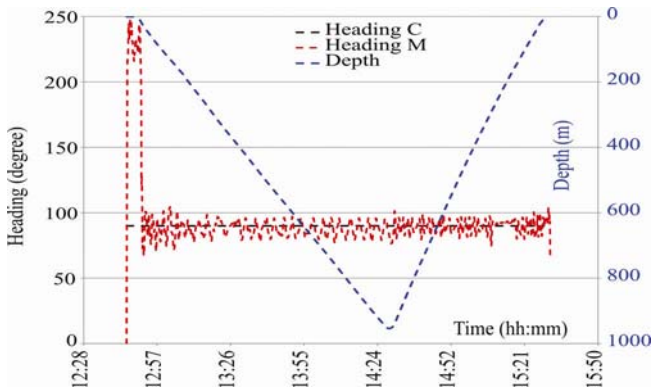


Figure 10. Commanded heading (Heading C), measured heading (Heading M) and depth (Depth) during the mission on 13 September 2013.

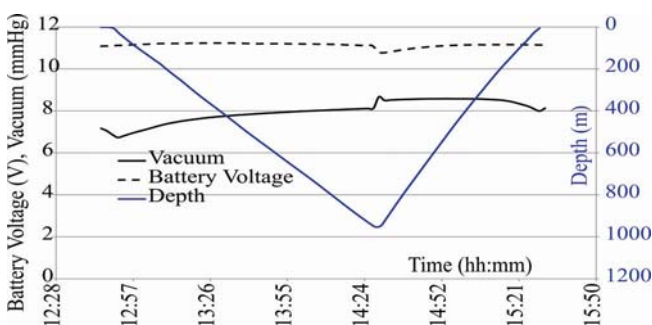


Figure 11. Internal vacuum and battery voltage during the mission on 13 September 2013.

position and attitude respectively. The rudder was operated in the positive side to counter deviation in the heading due to current. The rudder deflected (Figure 9) less in climbing than diving since the climb speed (0.26 m/s) was more than dive speed (0.16 m/s). The rudder movement was not saturated and the glider could continue the

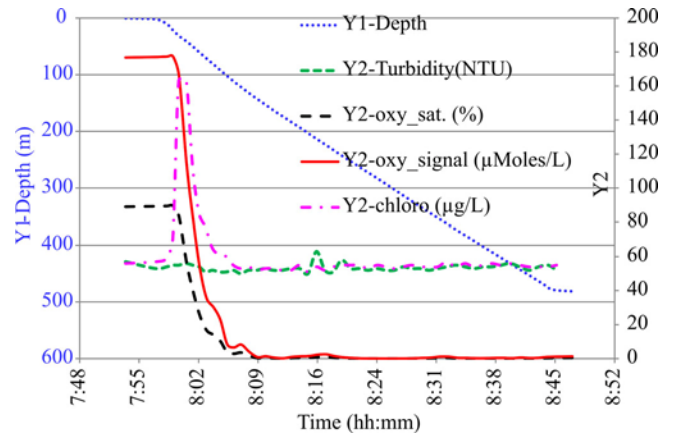


Figure 12. Optical sensors data recorded during 500 m profile on 15 September 2013 (Y1: depth, Y2: turbidity, oxygen saturation (oxy_sat.), oxygen signal (oxy_signal), chlorophyll (chloro)).

mission. It was observed that, below 100 m depth the glider maintained 70°–105° heading, with an average of 88° (Figure 10). When the oil pump worked at commanded depth the battery voltage was reduced to 10.77 V (Figure 11). The glider dived to 952.4 m depth and climbed to surface in 9874 s and navigated 3.4 km horizontally at 74° heading. The dive-time to climb-time ratio of 1.62 indicates that the glider is light.

Optical sensor data: The science computer on the glider collected data from optical sensors at 0.5 m depth interval. Figure 12 shows the optical sensors data recorded on 15 September 2013 in a 500 m dive at position 12.897°N, 84.138°E.

Comparison of conductivity and temperature sensors: The Barathi glider recorded temperature (T) and conductivity (C) profiles during the short-duration mission. These were compared with manually measured T and C profiles from a *ORV Sagar Manjusha* (Micro Star Plus, M/s Seabird Electronics Inc., USA). Table 2 gives the position and time details of the profiles. Data from B1 and S1 are linearly interpolated with 1 m resolution until 100 m depth. Data from B2 and S2 are linearly interpolated with 10 m resolution until 480 m depth. Table 3 shows the mean and standard deviation (SD) of the T and C profiles.

The root mean square deviation (RMSD) of temperature and conductivity profiles were computed (Table 4). It can be seen that RMSD of temperature and conductivity of

RESEARCH ARTICLES

B1 and S1 profiles are higher compared to B2 and S2 profiles due to upper layer variations.

Figures 13 and 14 show the scatter plots of temperature and conductivity profiles of B1 (B2) versus S1 (S2), respectively. Figures 15 and 16 show the scatter plots of temperature and conductivity profiles of B2 and S2 respectively. It is seen that temperature (B1 and S1, B2 and S2) and conductivity (B1 and S1, B2 and S2) profiles are strongly correlated (Table 5). Marginal differences in the upper layer measurements are due to time and positional differences that existed between the observations.

Long-duration mission

Trajectory: NIOT planned a four-month mission to sample central BoB with the glider Barathi. The glider was deployed from aft of ORV *Sagar Manjusha* at position 13.243°N, 80.700°E on 24 April 2014 at 7:30 h in 900 m ocean depth. The glider was piloted through Iridium satellite telemetry from the control room at NIOT with heading and way point based missions.

The glider Barathi reached at position 12.905°N, 86.291°E, 655 km away from Chennai coast on 9 June 2014 and changed its heading towards west. The glider Barathi had voyaged 850 km horizontally in 46 days till then. It consumed 34.7% energy and completed 1351 dives. The glider voyaged towards Chennai coast from 9

June 2014 to 28 August 2014. It was recovered by the Indian Coast Guard patrol vessel *Rani Abbakka*. Figure 15 shows the trajectory of the glider from 24 April to 28 August 2014. It consumed 81% energy and completed 3400 dives to voyage 2125 km.

Spatial variations of density and sound velocity along 13°N latitude and between 80.76°E and 86.25°E: The glider Barathi was programmed to record temperature and conductivity profiles during the mission. The temperature and conductivity profiles (G1–G12, Table 6) measured

Table 4. RMSD of temperature and conductivity profiles

Variable	Temperature profile		Conductivity profile	
	Ship cast 1	Ship cast 2	Ship cast 1	Ship cast 2
Barathi 1	0.47	–	0.063	–
Barathi 2	–	0.25	–	0.031

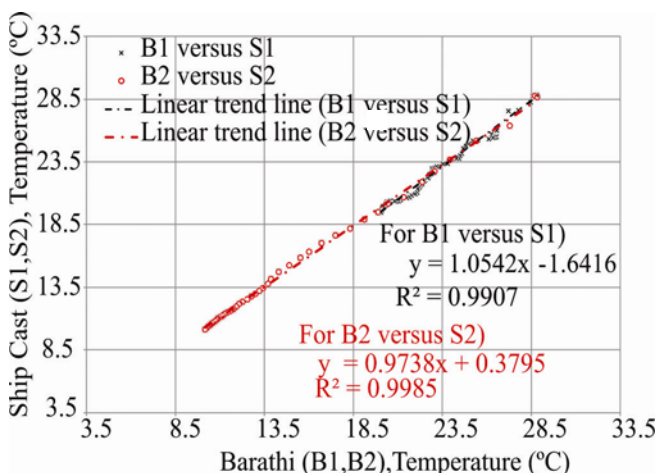


Figure 13. Scatter plot of the temperature profiles (B1, Barathi 1 versus S1, Ship cast 1 and B2, Barathi 2 versus S2, Ship cast 2).

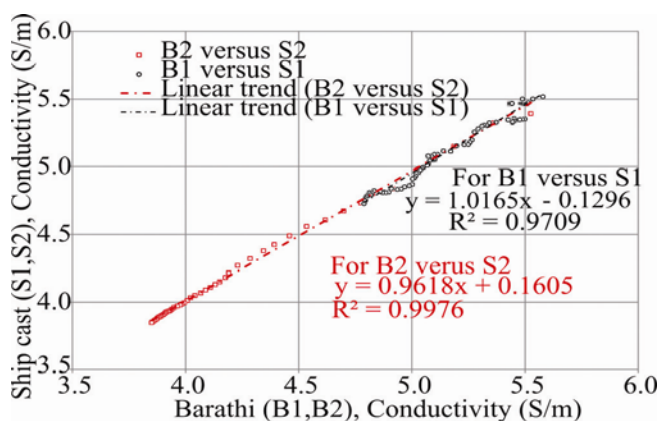


Figure 14. Scatter plot of the conductivity profiles (B1, Barathi 1 versus S1, Ship cast 1 and B2, Barathi 2 versus Ship cast 2).

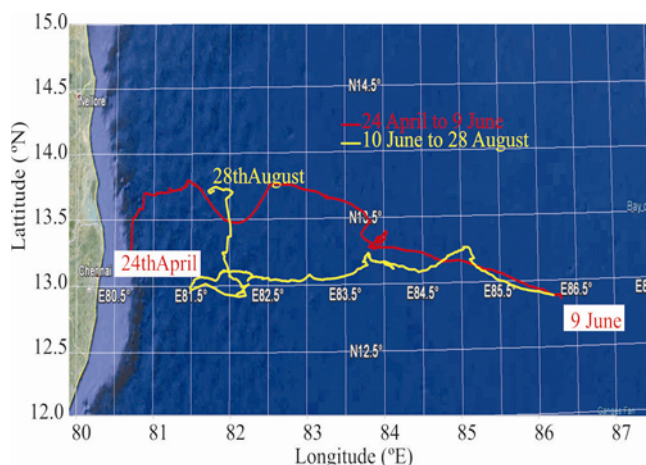


Figure 15. Trajectory of glider from 24 April to 28 August 2014.

Table 5. Coefficient of determination of temperature and conductivity profiles

Variable	Temperature profile		Conductivity profile	
	Ship cast 1	Ship cast 2	Ship cast 1	Ship cast 2
Barathi 1	0.9907	–	0.9709	–
Barathi 2	–	0.9985	–	0.9976

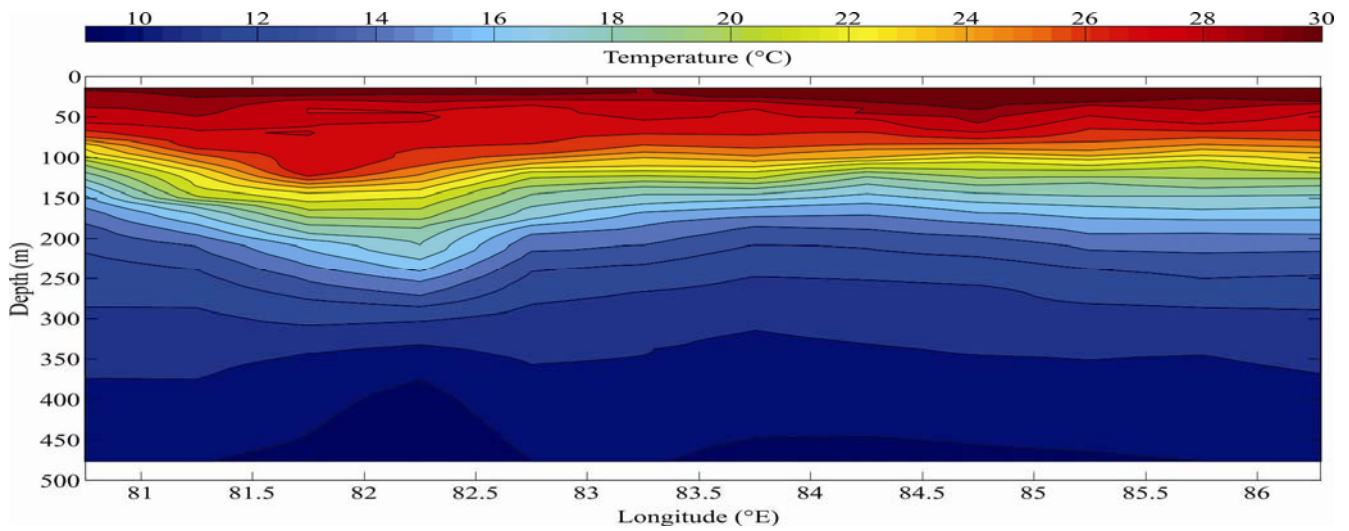


Figure 16. Depth-longitude section of temperature (contour interval: 1°C).

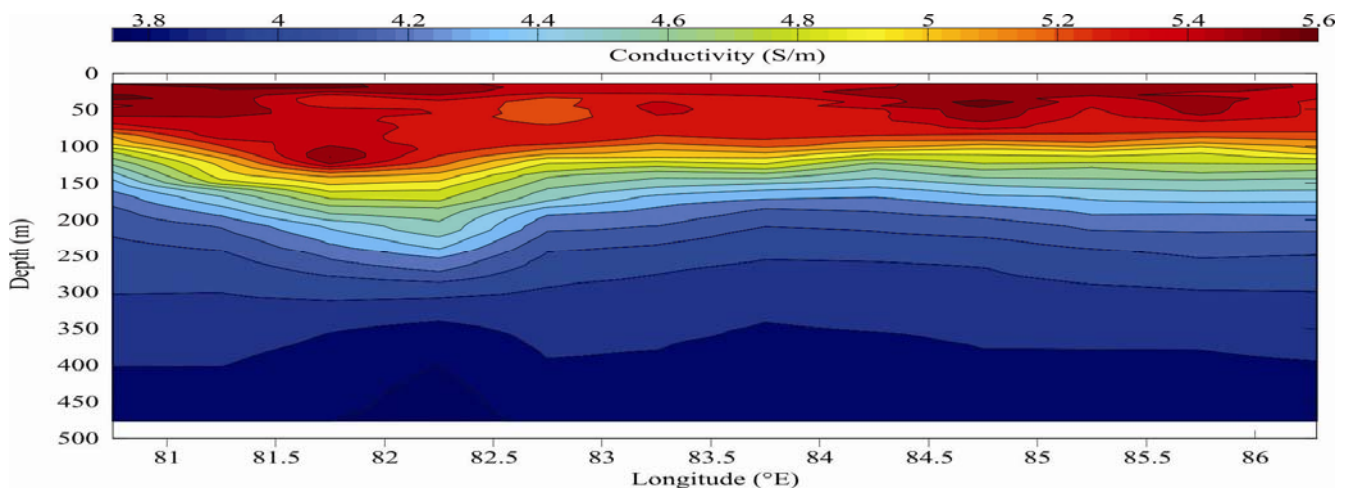


Figure 17. Depth-longitude section of conductivity (contour interval: 0.1 S/m).

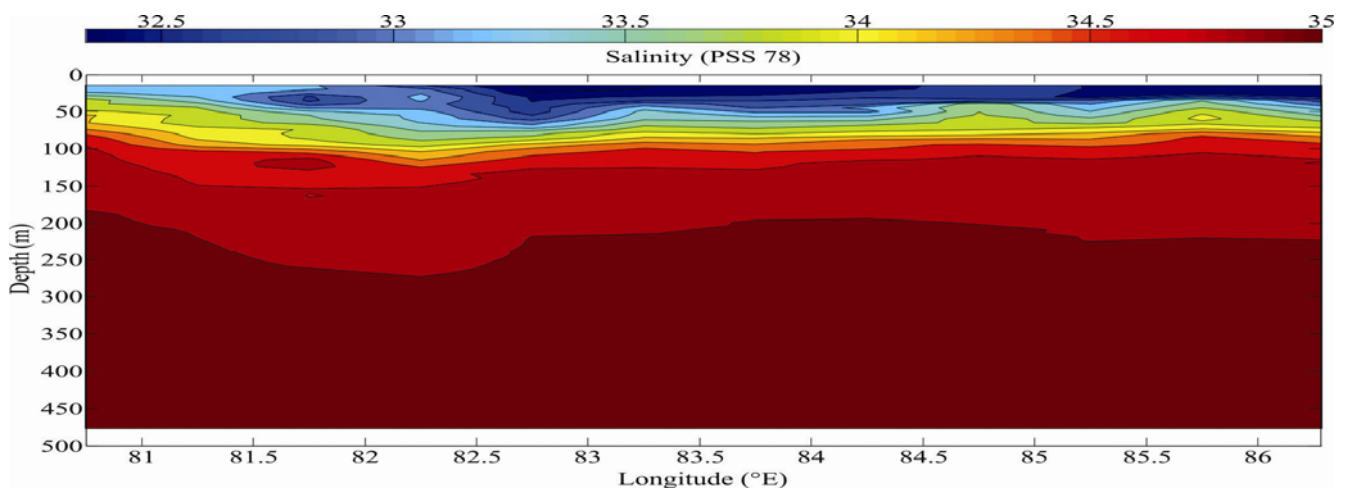


Figure 18. Depth-longitude section of salinity (contour interval: 0.2 PSS 78).

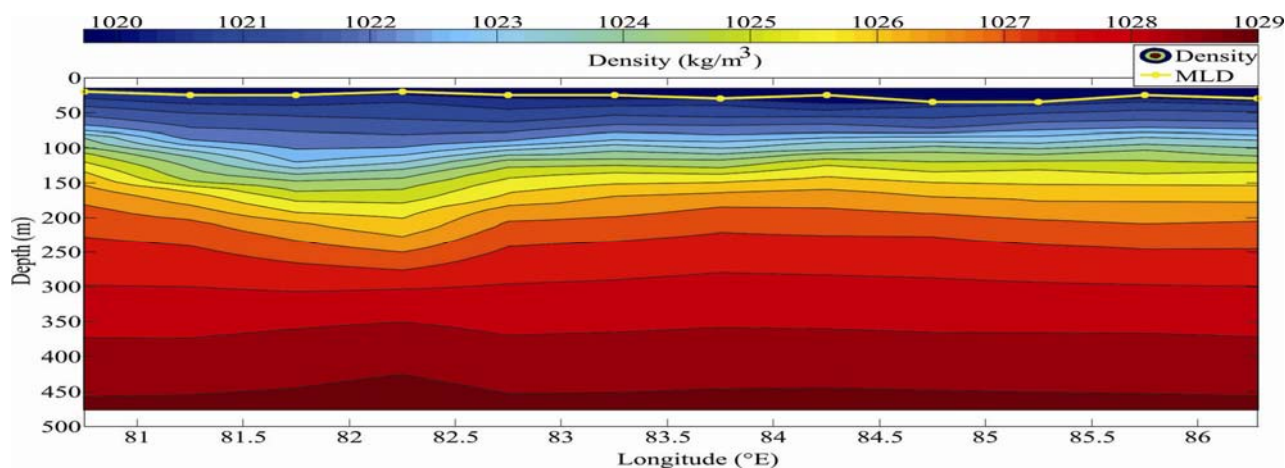


Figure 19. Depth-longitude section of density (contour interval: 0.5 kg/m³; yellow line, MLD).

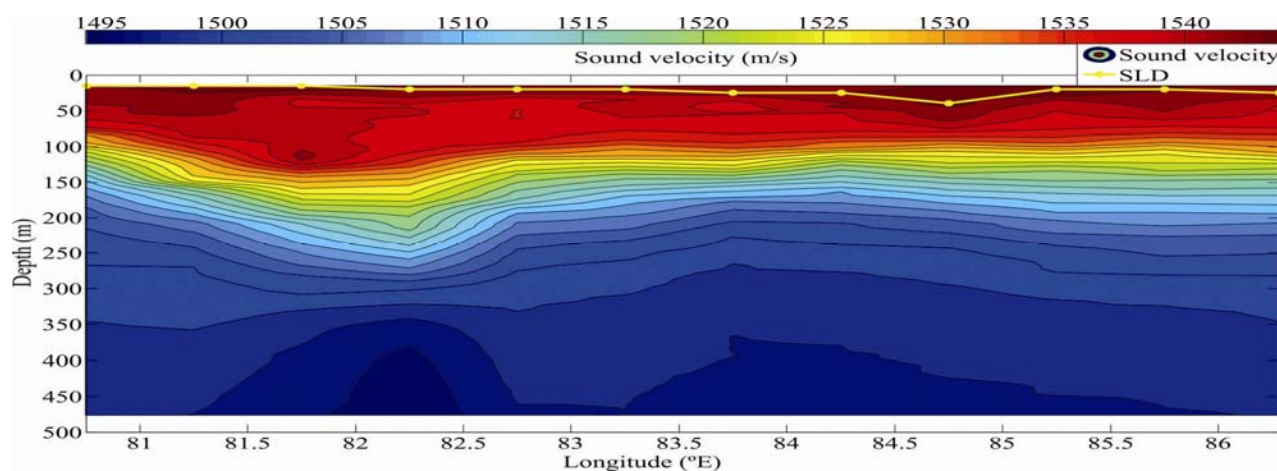


Figure 20. Depth-longitude section of sound velocity (contour intervals: 2 m/s; yellow line: SLD).

Table 6. Details of temperature and conductivity profiles

Station no.	Date, time	Position
G1	24 April 2014, 18:59:46	13.5263°N, 80.7620°E
G2	27 April 2014, 07:33:01	13.7294°N, 81.2406°E
G3	30 April 2014, 13:04:21	13.6728°N, 81.6909°E
G4	02 May 2014, 00:55:50	13.4823°N, 82.1221°E
G5	05 May 2014, 23:32:05	13.7656°N, 82.8363°E
G6	07 May 2014, 23:23:27	13.7022°N, 83.1761°E
G7	13 May 2014, 04:09:47	13.5173°N, 83.7743°E
G8	31 May 2014, 21:06:35	13.2730°N, 84.2456°E
G9	03 June 2014, 12:18:59	13.1822°N, 84.7590°E
G10	05 June 2014, 08:07:05	13.1396°N, 85.2496°E
G11	07 June 2014, 06:44:51	13.0255°N, 85.7665°E
G12	09 June 2014, 12:53:59	12.9341°N, 86.2841°E

between 80.76°E and 86.28°E long. and along 13.35°N (12.93–13.77°N) lat. from 24 April to 9 June 2014 are considered for the present study.

The data from G1 to G12 profiles were linearly interpolated at 5 m depth interval from 10 to 475 m depth. Figures 16 and 17 show the depth-longitude sections of temperature and conductivity respectively. The depth-

longitude section of the salinity (PSS78 scale, Figure 18), density (Figure 19) and sound velocity (Figure 20) profiles were computed from the pressure, temperature and conductivity profiles⁴⁴.

It can be seen that isotherm, isopycnal and sound velocity deepen between 81.75°N and 82.75°N (Figures 16, 19 and 20). In order to decipher this phenomenon, the sea-surface current from OSCAR forecast and SST from AVHRR data were analysed. The OSCAR forecast shows the presence of EICC of speed 0.47 m/s at 200° (0.82 m/s at 180°) at G1 (G2) station³⁰. The positions of G1 and G2 profiles are marked in the OSCAR forecast (Figure 21 a). Winds with a magnitude of 20–30 km/h prevailed towards northeast direction till 3 May 2014. SST on 27 April 2014 (Figure 21 b) shows that the southern part of the Bay was warmer compared to the northern part. The EICC carried warm water from the southern part of the Bay towards the northeastern direction and radiated there. The eddy centred at 15.30°N, 83.34°E supported the transportation of heat towards northeast. A near-shore salinity front (Figure 18) on the east coast of India is seen as a trace of the EICC^{10,56}.

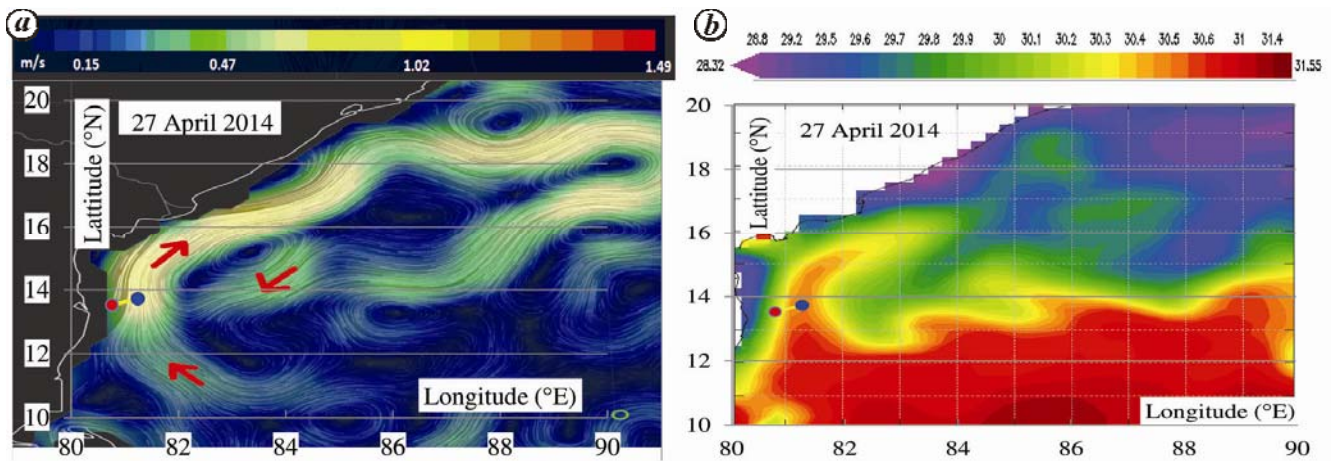


Figure 21. *a*, Sea-surface current on 27 April 2014 from OSCAR (Red arrow, Direction of the current; red dot, G1; blue dot, G2). *b*, sea-surface temperature (SST) on 27 April 2014 from AVHRR (Red dot, G1; blue dot, G2).

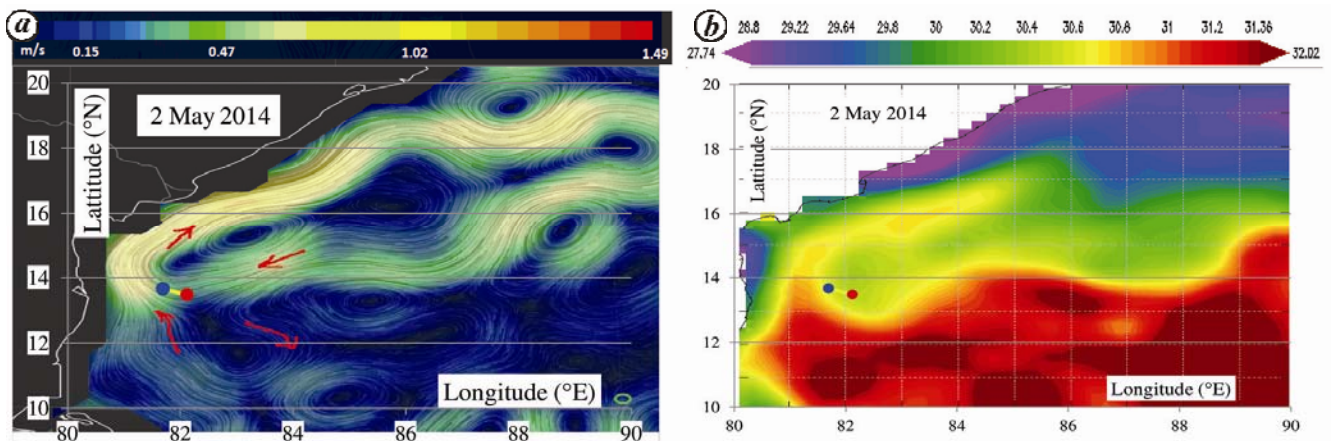


Figure 22. *a*, Sea-surface current on 2 May 2014 from OSCAR (Red arrow, Direction of the current; blue dot, G3; red dot, G4). *b*, SST on 2 May 2014 from AVHRR (Blue dot, G3; red dot, G4).

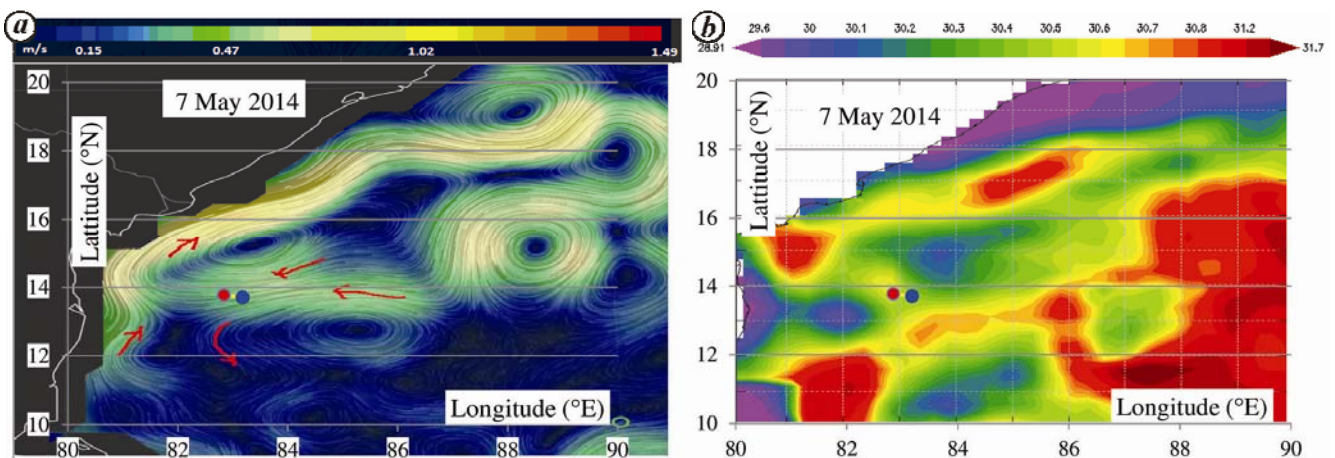


Figure 23. *a*, Sea-surface current on 7 May 2014 from OSCAR (Red arrow, direction of the current; red dot, G5; blue dot: G6). *b*, SST on 7 May 2014 from AVHRR (red dot, G5; blue dot, G6).

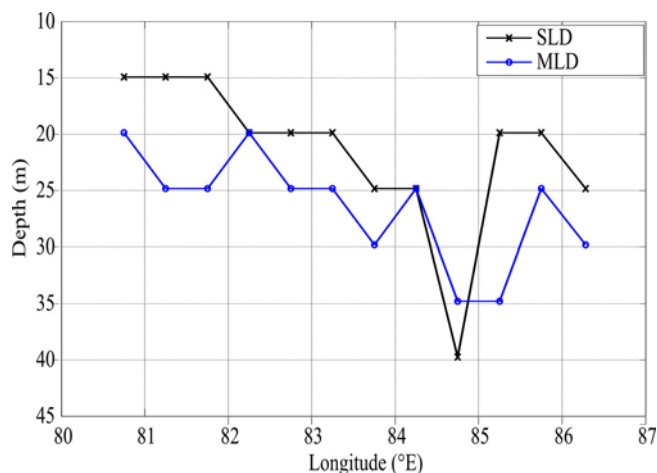


Figure 24. Depth-longitudinal variation of SLD and MLD.

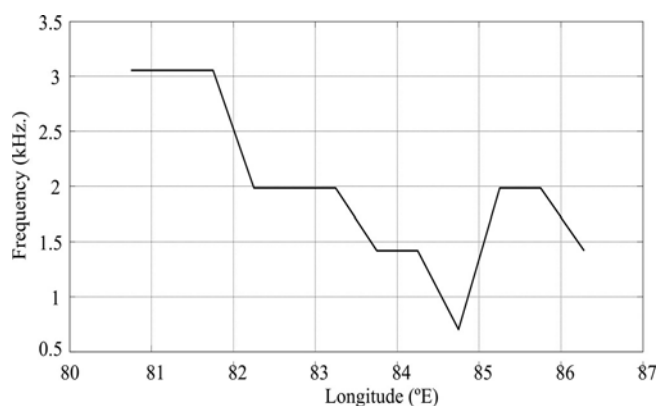


Figure 25. Depth-longitudinal variation of lower cutoff frequency.

Table 7. Statistical parameters of MLD and SLD

Parameter	MLD (m)	SLD (m)
Minimum	19.88	14.91
Maximum	34.80	39.77
Mean	26.51	21.54
SD	04.89	06.81

The intensity of EICC was reduced at G3 and G4 stations. Figure 22a shows the sea-surface current forecast on 2 May 2014 at G3 and G4 stations. The intensity of EICC is reduced to 0.58 m/s 165° (0.22 m/s 105°) at G3 (G4) station. The glider moved to cooler regions towards east (Figure 22b). Figure 23a and b shows the sea-surface current forecast and SST on 7 May 2014 respectively. It is seen that the surface current in the region is influenced by eddies at 12.92°N, 85.28°E (anti-clockwise) and 15.45°N, 83.48°E (clockwise). Two distinct warm water masses are seen at the surface in the northern Bay along the EICC path. The region around G5 station is warmer compared to G6 station and the same is seen in the glider observations.

MLD (Figure 19) was computed from the density profile. SLD (Figure 20) was computed from the sound

velocity profile. Table 7 shows the statistical parameters of MLD and SLD. It is seen that SLD (MLD) (Figure 24) increases from 15 m (20 m) near the coast to 25 m (30 m) in the central BoB. Even though there is a noticeable departure (>15 m) between SLD and MLD, occasionally they coincide. SLD deepened to 4.9 m more than MLD at 84.7590°E long on 3 June 2014.

The lower cutoff frequency (Figure 25) of the surface duct is calculated according to eq. (9); it ranges from 0.7 to 3.0 kHz.

Conclusion

In this article we have discussed ballasting procedure for operating a glider for long duration in highly variable sea-water conditions. Data from a short-duration mission in the BoB are presented. It is seen that below 100 m depth, fluctuation in heading is less compared to near the surface. Our temperature and conductivity data are strongly correlated (coefficient of determination $R^2 > 0.97$) with commercially available instruments. The 127 days mission of glider Barathi highlights the feasibility of operating gliders in the BoB with ± 2.6 N buoyancy variations. A near-shore salinity front in the east coast of India is seen as a trace of the EICC. It is seen that SLD (MLD) increases from 15 m (20 m) near the coast to 25 m (30 m) in the central BoB. The lower cutoff frequency of surface duct ranges from 0.7 to 3.0 kHz. The present study demonstrates utilization of a novel *in situ* observation platform, an underwater glider in the BoB.

A comprehensive time and spatial measurement using the glider network will certainly improve our understanding of the Indian Ocean and the surrounding regions.

1. http://www.nio.org/index?option=com_nomenu/task/show/tid/2/sid/18/id/5 (accessed on 6 October 2014).
2. Venkatesan, R., Shamji, V. R., Latha, G., Simi Mathew, Rao, R. R., Arul Muthiah, M. and Atmanand, M. A., *In situ* ocean subsurface time-series measurements from OMNI buoy network in the Bay of Bengal. *Curr. Sci.*, 2013, **104**(9), 1166–1177.
3. Venkatesan, R. *et al.*, Signatures of very severe cyclonic storm Phailin in met-ocean parameters observed by moored buoy network in the Bay of Bengal. *Curr. Sci.*, 2014, **107**(4), 589–595.
4. McPhaden, M. J. *et al.*, RAMA: The research moored array for African–Asian–Australian monsoon analysis and prediction. *Bull. Am. Meteorol. Soc.*, 2009, **90**, 459–480.
5. <http://www.aoml.noaa.gov/phod/goos/xbtscience/> (accessed on 6 October 2014).
6. Kent, E., Ball, G., Berry, D., Fletcher, J., North, S. and Woodruff, S., The Voluntary Observing Ship (VOS) scheme. In Proceedings of Ocean Obs'09: Sustained Ocean Observations and Information for Society Conference, Venice, Italy, ESA Publication, 2009, WPP-306; doi:10.5270/OceanObs09.cwp.48.
7. <http://www.incois.gov.in/argo/argo.jsp> (accessed on 6 October 2014).
8. Zuidema, P., Convective clouds over the Bay of Bengal. *Mon. Wea. Rev.*, 2003, **131**, 780–798.
9. Webster, P. J. *et al.*, The JASMINE pilot study. *Bull. Am. Meteorol. Soc.*, 2002, **83**, 1603–1630.
10. Shenoi, S. S. C., Intra-seasonal variability of the coastal currents around India: a review of the evidences from new observations. *Indian J. Mar. Sci.*, 2010, **39**(4), 489–496.

11. <http://www.ioos.noaa.gov/glider/welcome.html> (accessed on 6 October 2014).
12. Stommel, H., The Slocum mission. *Oceanography*, 1989, **2**, 22–25.
13. Bachmayer, R., Leonard, N. E., Graver, J., Fiorelli, E., Batha, P. and Palley, D., Underwater gliders: recent developments and future applications. In Proceeding of IEEE International Symposium on Underwater Technology, Taipei, Taiwan, 2004.
14. Rudnick, D. L., Davies, R. E., Eriksen, C. C., Fratantoni, D. M. and Perry, M. J., Underwater gliders for ocean research. *J. Mar. Technol. Soc.*, 2004, **38**, 73–84.
15. Testor, P. *et al.*, Gliders as a component of future observing systems. In Proceedings of the Ocean Obs'09: Sustained Ocean Observations and Information for Society Conference, Venice, Italy, 2009.
16. <http://www.webbresearch.com/pdf/SlocumGlider.pdf> (accessed on 6 October 2014).
17. http://auvac.org/uploads/configuration_spec_sheets/Slocum%20-Endurance%202009.pdf (accessed on 8 August 2014).
18. <http://www.webbresearch.com/pdf/EurekaMoment.pdf> (accessed 27 June 2014).
19. Glenn, S., The Trans-Atlantic Slocum glider expeditions: a catalyst for undergraduate participation in ocean science and technology. *Mar. Technol. Soc. J.*, 2011, **45**(1), 52–67.
20. <https://datahost.webbresearch.com/files.php?cwd=/glider/production/doco/MANUAL> (accessed on 27 June 2014).
21. Davis, R. E., Eriksen, C. C. and Jones, C. P., Technology and applications of autonomous underwater vehicles. In *Technology and Applications of Autonomous Underwater Vehicles* (ed. Griffiths, G.), Taylor and Francis, London, 2003, pp. 37–58.
22. Webb, D. C., Simonetti, P. J. and Jones, C. P., SLOCUM: An underwater glider propelled by environmental energy. *IEEE J. Ocean Eng.*, 2001, **26**(4), 447–452.
23. Eriksen, C. C. *et al.*, Sea glider: a long-range autonomous underwater vehicle for oceanographic research. *IEEE J. Ocean. Eng.*, 2001, **26**(4), 424–436.
24. http://www.acsa-alcen.com/sites/acsa-alcen.com/files/datasheet/acsa_seaexplorer_datasheet.pdf (accessed on 6 February 2015).
25. http://auvac.org/uploads/platform_pdf/Bluefin-Spray-Glider-Product-Sheet.pdf (accessed on 6 February 2015).
26. Sherman, J., Davis, R., Owens, W. B. and Valdes, J., The autonomous underwater glider 'Spray'. *IEEE J. Ocean. Eng.*, 2001, **26**(4), 437–446.
27. Roemmich, D. *et al.*, Integrating the ocean observing system: mobile platforms. In Proceedings of the Ocean Obs'09: Sustained Ocean Observations and Information for Society Conference, Venice, Italy, 2009.
28. http://www.ioos.noaa.gov/observing/observing_assets/glider_asset_map.html (accessed on 6 February 2015).
29. <http://marine.rutgers.edu/cool/auvs/> (accessed on 6 February 2015).
30. <http://www.incois.gov.in/portal/datainfo/insituhome.jsp> (accessed on 6 February 2015).
31. Ravichandran, M., Vinayachandran, P. N., Sudheer, J. and Radhakrishnan, K., Results from first ARGO float deployed by India. *Curr. Sci.*, 2004, **86**(5), 651–659.
32. http://www.jamstec.go.jp/ARGO/argo-web/results/system_building/deployment/weight_adjustment/TR-ballasting2.pdf (accessed on 1 May 2015).
33. Kobayahi, T. *et al.*, Quality control of Argo Data Based on high quality climatological dataset (HydroBase) I; http://www.jamstec.go.jp/ARGO/argo_web/results/data_management/management/quality_control_1/Quality_control.pdf (accessed on 19 January 2015).
34. Shankar, D., McCreary, J. P., Han, W. and Shetye, S. R., Dynamics of the East India Coastal Current: 1. Analytic solutions forced by interior Ekman pumping and local alongshore winds. *J. Geophys. Res. C6*, 1996, **101**, 13975–13991.
35. Varkey, M. J., Murty, V. S. N. and Suryanarayana, A., Physical oceanography of the Bay of Bengal and Andaman Sea. In *Oceanography and Marine Biology: Annual Review* (eds Ansell, A. D., Gibson, R. N. and Barnes, M.), UCL Press, London, UK, 1996, vol. 34, pp. 1–70.
36. Murty, V. S. N., Sarma, Y. V. B., Babu, M. T. and Rao, D. P., Hydrography and circulation in the northwestern Bay of Bengal during the retreat of southwest monsoon. *Proc. Indian Acad. Sci. (Earth Planet. Sci.)*, 1992, **101**, 67–75.
37. Vinayachandran, P. N. and Kurian, J., Modeling of Bengal Fresh Plume and Arabian Sea Mini Warm Pool. In Proceedings of the 12th Asian Congress of Fluid Mechanics, Daejeon, Korea, 2008, pp. 1–5.
38. Vinayachandran P. N. and Kurian, J., Hydrographic observations and model simulations of the Bay of Bengal freshwater plume. *Deep Sea Res. I*, 2007, **54**, 471–486.
39. Sengupta, D. and Ravichandran, M., Oscillations of Bay of Bengal sea surface temperature during the 1998 summer monsoon. *Geophys. Res. Lett.*, 2001, **28**(10), 2033–2036.
40. Vinayachandran, P. N., Neema, C. P., Simi, M. and Remya, R., Mechanisms of summer intraseasonal sea surface temperature oscillations in the Bay of Bengal. *J. Geophys. Res.*, 2012, **117**, C01005.
41. <http://las.incois.gov.in/las/UI.vm> (accessed on 4 March 2014).
42. Millero, F. J. and Huang, F., The density of seawater as a function of salinity (5 to 70 g kg⁻¹) and temperature (273.15 to 363.15 K). *Ocean Sci.*, 2009, **5**, 91–100.
43. Frank, J. M. and Alain, P., International one-atmosphere equation of state of seawater. *Deep-Sea Res.*, 1981, **28**(6), 625–629.
44. www.TEOS-10.org (accessed on 4 March 2014).
45. http://www.nodc.noaa.gov/argo/floats_data.htm (accessed on 4 March 2014).
46. Bansal, R. K., *Fluid Mechanics*, Laxmi Publications (P) Ltd, New Delhi, 2008, pp. 137–138.
47. Som, S. K. and Biswas, G., In *Introduction to Fluid Mechanics and Fluid Machines*, Tata McGraw-Hill, New Delhi, 1998, pp. 46–52.
48. Ohno, Y., Kobayashi, T., Iwasaka, N. and Suga, T., The mixed layer depth in the North Pacific as detected by the Argo floats. *Geophys. Res. Lett.*, 2004, **L1306**.
49. Udaya, B., T. V. S., Swain, D. and Ravichandran, M., Inferring mixed-layer depth variability from Argo observations in the western Indian Ocean. *J. Mar. Res.*, 2006, **64**, 393–406.
50. Fofonoff, P. and Millard Jr, R. C., Algorithms for computation of fundamental properties of seawater. UNESCO Technical Papers in Marine Science, 1983, vol. 44, pp. 46–49.
51. Etter, C. P., *Underwater Acoustic Modelling: Principles, Techniques and Applications*, E&FN Spon, London, 1996, 2nd edn, pp. 82–83.
52. Jain, S., Ali, M. M. and Sen, P. N., Estimation of sonic layer depth from surface parameters. *Geophys. Res. Lett.*, 2007, **34**, L17602.
53. Urlick, R. J., *Principles of Underwater Sound*, McGraw-Hill, New York, USA, 1983, 3rd edn, p. 423.
54. <http://earth.nullschool.net/> (accessed on 6 October 2014).
55. <http://ferret.pmel.noaa.gov/Ferret/LAS/home/> (accessed on 6 October 2014).
56. Shetye, S. R., Shenoi, S. S. C., Gouveia, A. D., Michael, G. S., Sundar, D. and Nampoothiri, G., Wind-driven coastal upwelling along the western boundary of the Bay of Bengal during the southwest monsoon. *Cont. Shelf Res.*, 1991, **11**, 1397–1408.

ACKNOWLEDGEMENTS. We thank the Ministry of Earth Sciences, Government of India for funds; the Vessel Management Group, NIOT Chennai for providing ship for deployment and the Indian Coast Guard for recovery of the glider. We also thank the Ocean Electronic Department, NIOT for active support during deployment operations; Teledyne Webb Research Corporation, USA, supplying the glider and for technical support; the Earth and Space Research Institute, USA, for easy access to ocean surface current forecast OSCAR, and the Indian National Centre for Ocean Information Services, Hyderabad, for providing AVHRR and Argo data service in Live Access Server.

Received 19 January 2015; revised accepted 25 May 2015